CSIRO PUBLISHING

International Journal of Wildland Fire **2011**, *20*, 384–393 www.publish.csiro.au/journals/ijwf

Numerical modelling of the aerial drop of firefighting agents by fixed-wing aircraft. Part I: model development

J. H. Amorim

Centre for Environmental and Marine Studies (CESAM), Department of Environment and Planning, University of Aveiro, 3810-193 Aveiro, Portugal. Email: amorim@ua.pt

Abstract. The efficiency of the aerial drop of firefighting agents (water and retardants) is extremely dependent on pilot skills in dealing with complex atmospheric conditions, mostly because on-board systems for computer-assisted drops have not yet been used operationally. Hence, numerical modelling tools can be of primary importance for the optimisation of firefighting operations and in the testing of new chemical products. The current work addresses the development of the operational Aerial Drop Model. This numerical tool allows a near real-time simulation of aerial drops with fixed-wing aircraft, while covering the fundamental stages of the process. It copes with a wide range of product viscosities, from water to highly thickened long-term retardants. The Aerial Drop Model simulates the continuous stripping of droplets from the liquid jet by the action of Rayleigh–Taylor and Kelvin–Helmholtz instabilities applying the linear stability theory. The subsequent secondary breakup and deformation of the formed droplets due to aerodynamic forces is based on experimental correlations defined in terms of the dimensionless Weber number. Droplet trajectories are computed by applying a Lagrangian approach, in which a dynamical drag module accounts for the effect of deformation. This operational tool provides an improved understanding of the behaviour and effectiveness of aerially delivered firefighting liquids.

Additional keywords: drop effectiveness, droplet flow, forest fires.

Introduction and background

The World Health Organization (WHO 2007) has identified forest fires as one of the threats to public health security in the 21st century, and climate change has been positively linked to an increase in the frequency and severity of forest fires (Westerling *et al*. 2006; IPCC 2007). Aerial application of firefighting products plays an important role in protecting human lives and patrimony from wildfires, and its importance is likely to increase as wildfire severity increases. In fact, aircraft use against wildfires has increased since the 1960s, especially in the United States, Australia and several European countries, in particular Greece and France. If integrated into an effective global strategy, aircraft can play an important role in wildfire management, especially in situations requiring rapid intervention, such as emerging fires, inaccessible mountainous areas, or other high-risk situations.

The efficiency of the aerial drop of firefighting liquids is determined by the application of the product in the correct spot and in the quantity most adequate for retarding or extinguishing the fire front, and permitting the subsequent attack by ground resources. However, as the factors that determine drop efficiency are numerous, without the use of operational decision-support systems (DSS), this is potentially an operation with unpredictable results, highly dependent on the skills of the pilot. The use of modelling tools that can aid the pilot's decision on the best way to conduct the drop can be of primary importance during firefighting or training operations.

Despite the development of powerful numerical codes for fluid dynamics modelling, associated with the rapid growth of hardware performance, it is still difficult to determine the ground distribution of the applied liquid, even though the parameters affecting drop performance and ground distribution are known (Giménez *et al*. 2004). The complexity inherent in the numerical simulation of this process results mostly from the panoply of dynamic phenomena that contribute to the breakup of the bulk liquid, i.e. the dynamical transition into droplets of varying dimensions, and also in the following drift and deposition of the formed droplets. These factors will ultimately determine the coating of the fuel by the product and the characteristics of the ground pattern, including the position of the pattern in relation to the target, the length and area of each coverage level and the volume of drifted agent.

Under this scope, the objective of the current work was the development (Part I) and validation (Part II, Amorim 2011) of the operational Aerial Drop Model (ADM), which is intended for the simulation of the spatiotemporal behaviour of firefighting liquid agents (water and retardants) in the atmosphere and the resulting coverage pattern of the ground surface. ADM was designed to cover the main stages involved, namely: (1) the outflow of the liquid from the aircraft tank; (2) the two-stage liquid breakup; (3) the droplet shape distortion and gravitational settling; and (4) the ground deposition of the spray cloud. Whereas Part I, the current document, is dedicated to the development of the model, Part II (Amorim 2011) describes the comparison of modelling results with a set of real-scale drop tests, in which a wide range of operational conditions were analysed, including different delivery system types, flight parameters, meteorological conditions and product characteristics.

 10.1071/WF09122 1049-8001/11/030384

Fig. 1. Schematic representation (George and Blakely 1973) and sequence of images of a retardant aerial drop (Blodgett Fire (US), August 2000). (Scale: 1 foot = 0.30 m.) (Photo credit: Bruce Weide (Wild Sentry, Hamilton, MT).)

Literature review on the numerical modelling of the aerial drop of firefighting liquids

During an aerial drop, the liquid undergoes a complex sequence of dynamic mechanisms, as shown by Andersen *et al*. (1974*a*, 1974*b*, 1976). The first stage starts with the release of the firefighting agent from the tank. Depending on the tank's volume, the number of compartments opened simultaneously and the type of delivery system, the time for total efflux of conventional non-pressurised systems can typically take between 0.5 and 2 s for a dropped volume of ~5000 L, whereas in constant-flow systems, it can easily increase to 5 s or more. The geometrical characteristics of the tank and the doors' opening rate shape the emerging fluid in the first milliseconds of the drop.

As a result of the relative velocity between the emerging liquid and the atmosphere it enters (which at this stage is typically in the range from 50 to 70 m s^{-1}), the jet column of bulk liquid bends and deforms through thinning and lateral spreading. The increase of the frontal cross section of the jet column is, therefore, a result of the balance of aerodynamic drag, liquid inertia, gravity, surface tension, and viscous forces. Simultaneously, the bulk product undergoes a sequence of complex breakup mechanisms, which start with the continuous stripping of droplets from the liquid surface due to Rayleigh–Taylor and Kelvin–Helmholtz instabilities. This process produces a cascade of fluid structures that form a spray region with the characteristic cloud shape shown in the different stages of Fig. 1. The aerodynamic breakup of liquid jets is, in fact, a two-stage process composed of the primary breakup of the jet into large droplets (or globs) and the subsequent secondary breakup of these fluid structures with the formation of the spray cloud. After being formed, droplets are entrained in the wake flow that develops behind the liquid column, as found in other studies on the primary breakup of liquid jets (e.g. Linne *et al*. 2005). In this process, the smaller droplets resulting from the atomisation of the column in the first instants of the drop are also affected by the aircraft wake (generated by the fuselage and propellers). But as the droplet inertia is the determinant factor on the effect of the aircraft wake over the trajectory of the cloud, this effect is more relevant for pressurised aerial delivery systems than for conventional or constant-flow ones. Droplet dynamics within the gaseous flow is then governed by the interaction between the droplets (influenced by their size and shape) and the airflow, which results in a drag-induced deceleration. Finally, the gravitational settling of the liquid culminates with the penetration and coating of the canopy and the ground deposition of the remaining material not retained by the leaves and branches.

The breakup (or atomisation) is, in fact, the most important process controlling the behaviour of the product in the atmosphere, because it determines the size, velocity and location of the formed droplets. This will ultimately control the ground pattern of the product and the overall effectiveness of the drop. Hence, it is of major importance to pursue an accurate numerical description of the breakup stage, even in operational fast-running models. However, few attempts have succeeded in predicting, either experimentally or numerically, the complex process firefighting products (especially retardants) undergo when exposed to aerodynamic breakup, and the consequences on size distribution of droplets and final ground deposition.

The first and most detailed study on the breakup of firefighting liquids was undertaken by the Shock Hydrodynamics Division, from the Whittaker Corporation (California, US), under contract to the Intermountain Forest and Range Experiment Station of the US Forest Service (USDA-FS). These works, published in the mid-70s by Andersen *et al*. (1974*a*, 1974*b*, 1976), represent an important step forward on the understanding of the relation between the rheological characteristics of the products and aerial delivery performance. From this extensive work, significant relevance should be attributed to the

Table 1. Time chart of the numerical models developed or applied in the context of the aerial drop of firefighting products

Model	Characteristics	Reference
PATSIM	Empirical breakup module. Simplified wind flow	Swanson *et al*. (1975, 1977, 1978)
FARSITE	Decision support system for fire growth simulation. User-defined coverage levels. No drop-modelling capabilities	Finney (1998)
FireDrop	Intended for helicopter releases	Teske *et al*. (1999)
Fluent (volume-of-fluid method)	Attempt to numerically describe the breakup process. No validation	Rimbert *et al*. (2002)
RAM (retardant application model)	Applies PATSIM's empirical breakup module. Lagrangian trajectory. Graphical user interface	Tomé and Borrego (2002), Amorim *et al*. (2006)
FLUENT (Lagrangian method)	Applies PATSIM's empirical breakup module. Two-way coupling analysis	Tomé (2004)

shock-tube studies performed with the aim of obtaining a high-speed photographic coverage of the aerodynamic breakup of individual droplets and liquid jets of different retardant formulations and plain water. It was shown that effective viscosity, which is affected by the addition of the thickener to the retardant solution, contributes to the control of the terminal size of droplets produced by aerodynamic breakup.

The acquired knowledge and the extensive set of data compiled and analysed during the High-Altitude Drop Mechanisation (HADM) Study conducted by Honeywell Corporation under contract to the USDA-FS supported the development of the retardant ground pattern operational model PATSIM (PATtern SIMulation), a model capable of predicting retardant ground patterns over a range of aircraft velocities and altitudes (Swanson and Helvig 1973, 1974; Swanson *et al*. 1975, 1977, 1978). Later on, PATSIM was further tested by George and Johnson (1990).

In Europe, the most systematic investigation of the utilisation of retardants in fire prevention and suppression was conducted in the scientific projects ACRE (Additifs Chimiques Rheologie Evaluation) and ERAS (Extension Retardant Application System), both with financial support from the European Commission (EC). These projects supported the development and testing of the Retardant Application Model (RAM), which applies the empirical concept of the atomisation introduced in PATSIM plus some improvements at the level of the wind-flow description (Tomé and Borrego 2002; Amorim *et al*. 2006).

Based on the numerical simulation of deposition and drift of aerially applied pesticides in agriculture, Teske *et al*. (1999) developed, under contract to the USDA-FS, the FireDrop model for the prediction of the ground deposition distribution of fire retardants released from helicopters. This model is partly based on the Lagrangian trajectory model AgDRIFT (Teske *et al*. 1997).

PATSIM, RAM and FireDrop were all developed with the objective of having fast-running operational tools to be used in the optimisation of aerial delivery effectiveness. More detailed codes, like Computational Fluid Dynamics (CFD) models, have also been applied to the simulation of the behaviour of retardants in the atmosphere. Aiming to evaluate the interactions between the product cloud and the flow field, Tomé (2004) applied a two-way coupling scheme available in the commercial CFD model FLUENT. This work kept the original description of the spatio-temporal evolution of the breakup process as given by PATSIM, which provides only an empirical model for the estimation of the formation rate of droplets without information related to size distributions and velocities after breakup. In order to have a more physically based description of the spatiotemporal evolution of the breakup process, Rimbert *et al*. (2002) applied, under the scope of the EC Project ERAS, the Volume-of-Fluid (VOF) module from the FLUENT package, however without validation with measured data. This work was extended with the mathematical derivation of a set of closures for modelling two-phase flows (Séro-Guillaume and Rimbert 2005). However, and according to the authors, some of the coefficients in the closure relations are unknown, and thus need to be determined by experimental or numerical procedures in order to be applied to the numerical modelling of the aerial drop of firefighting products.

An interesting example of the potential use of aerial drop models for firefighting operations is given by the fire growth simulation model FARSITE (Finney 1998), in which a specific module of aerial attack allows the allocation of a set of air resources to a specific fire. However, the software does not have the capability to simulate the physical process of dropping; instead, the user is responsible for providing realistic efficiency parameters, such as the length of effective product pattern for different coverage levels, which means that the performance of this tool is extremely dependent on the accuracy of the data provided by the user. Nevertheless, the information provided by the numerical system can be useful to professional wildland fire planners and managers.

In conclusion, Table 1 summarises the most important numerical models related to the simulation of the aerial drop of firefighting liquids.

Development of the Aerial Drop Model

This section describes the general structure of the model, the most relevant input and output data, and the numerical approaches implemented in the code in order to deal with the physical phenomena describing the aerial drop of firefighting liquids. A detailed description of the model can be found in Amorim (2008).

General description and structure

In terms of internal structure, the model is divided into four modules, as represented in Fig. 2, plus an additional one that

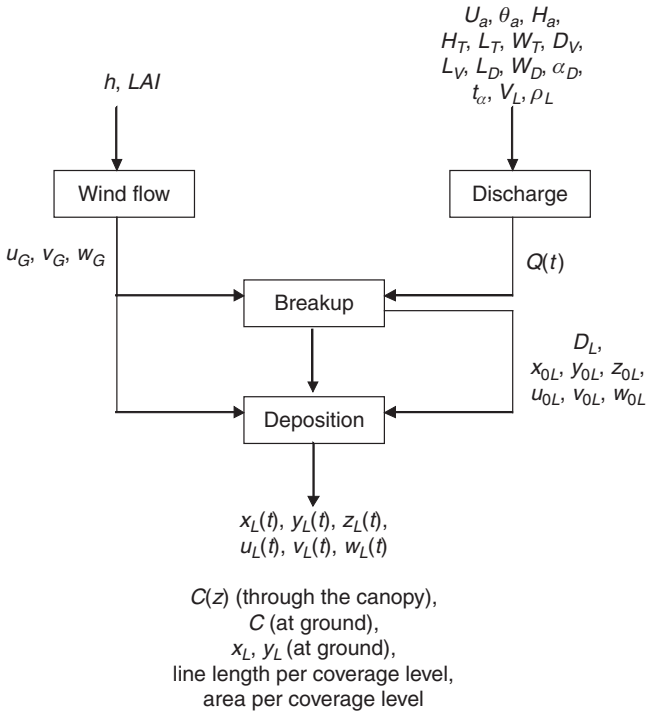

Fig. 2. General fluxogram of Aerial Drop Model (ADM) showing the different modules and main data flow. See Table 2 and the Appendix for the definition of variables.

calculates the metrics of interest and generates the output files. In the wind-flow module, the gas phase is modelled through a vegetative canopy model coupled to a modified surface-layer model adapted to cope with diabatic conditions. For the particulate phase, the primary breakup of the retardant jet is simulated in the breakup module through the application of the jet stability theory, which considers the continuous stripping of droplets due to the action of Rayleigh–Taylor and Kelvin–Helmholtz instabilities. This module runs in parallel with the deposition module, allowing the simulation of the motion and distortion of the formed droplets applying a Lagrangian approach, whereas the secondary breakup due to the aerodynamic forces is calculated based on experimental correlations defined in terms of the Weber number. A more detailed description of each module will be given hereafter.

ADM is written in the Fortran programming language. It is a fast running model that requires ~1 min CPU time on a current personal computer (e.g. 3-GHz processor and 2-GB memory) for completing a typical simulation. Calculations are made with a time-step of 0.02 s that supports a sufficiently detailed description of the entire process.

Input and output data

ADM requires only one input file in which the user provides all the parameters needed for the simulation. Some of these are already defined as default values that can be modified depending on the information available. The input data are shown in Table 2; although these are listed according to the different modules, they can be categorised in terms of product characteristics, operating flight conditions and meteorology.

Table 2. Input parameters used by Aerial Drop Model (ADM) model

Input parameters		Units
Wind flow module		
LAI	Leaf area index	$m^2\,m^{-2}$
h	Canopy height	m
U_m	Reference wind velocity	$m\,s^{-1}$
θ_m	Reference wind direction	°
H_m	Reference height	m
Discharge module		
H_T	Tank depth	m
L_T	Tank length	m
W_T	Tank width	m
D_V	Equivalent vent diameter	m
L_V	Vent length	m
L_D	Door length	m
W_D	Door width	m
α_D	Door opening angle	°
t_α	Door opening time	s
V_L	Volume dropped	L
ρ_L	Retardant density	$kg\,m^{-3}$
Breakup module		
μ_L	Retardant viscosity	cP
U_a	Aircraft velocity	$m\,s^{-1}$
θ_a	Aircraft direction	°
H_a	Drop height	m

The main output file provides the ground pattern of liquid in the form of liquid concentration per computational cell, allowing subsequent representation with surface mapping and contouring software. ADM also calculates the metrics of interest most commonly used in the evaluation of drop effectiveness: the length and area of the ground pattern. In order to support a more detailed analysis, these metrics are calculated for a given number of coverage levels, each one representing a given concentration range. During the calculation, the model also provides several other parameters: the volume of liquid atomised per unit of time, the diameter of droplets formed at each computational time-step, and the evolution with time of the 3-D position of droplets.

Wind flow

The unified theory from Harman and Finnigan (2007) for the description of the mean wind speed vertical profile in the presence of a vegetative canopy under varying atmospheric stability conditions served as the basis for the development of the ADM wind-flow module. It describes the flow inside the canopy and in the roughness sublayer (RSL) through the mixing layer analogy originally proposed by Finnigan (2000). For simplicity of the mathematical derivation, the vertical origin ($z = 0$) of the coordinate system was displaced to the canopy top. The modified displacement height (d_t) is related to the conventionally defined one (d) through the canopy height (h) according to:

$$d_t = h - d \tag{1}$$

Aligning the x axis with the mean wind, the vertical profile dU/dz where U is the mean wind speed, describing the air flow

Table 3. Reference leaf area index (*LAI*) values (means and standard deviations (s.d.) ($m^2\,m^{-2}$)) for distinct categories of vegetative canopies

Biome	Mean	s.d.
Crops	3.6	2.1
Grasslands	1.7	1.2
Managed forests of temperate deciduous broadleaf, temperate evergreen needleleaf and tropical deciduous broadleaf	8.7	4.3
Shrublands	2.1	1.6
Deciduous needleleaf forest	4.6	2.4
Deciduous broadleaf forest	5.1	1.6
Evergreen needleleaf forest	5.5	3.4

within the canopy ($z<0$) is calculated applying the known exponential formulation from Inoue (1963):

$$U(z) = U_h e^{\frac{z}{2\beta^2 L_c}} \quad (\text{for } z < 0) \tag{2}$$

For details about the closure expression applied in the calculation of the coefficient β, which relates the wind speed at the canopy top (U_h) to the friction velocity (u_*) for the flow in the overlying surface layer, see Harman and Finnigan (2007). Eqn 2 is given here in terms of the canopy-drag length scale L_c, which determines the efficiency of the canopy to remove momentum from the flow and, thus, is related to the distance required for the adjustment of the boundary layer to the canopy (Finnigan and Brunet 1995; Belcher *et al*. 2003). The approximate value of L_c can be calculated as follows:

$$L_c \approx \frac{h}{c_D LAI} \tag{3}$$

where c_D is the drag coefficient, which links the canopy architecture to its aerodynamic behaviour. For simplicity, a constant value of $c_D = 0.25$ is considered in the entire canopy depth, according to research by Cescatti and Marcolla (2004) and Novak *et al*. (2000). The leaf area index (*LAI*), however, is defined as one-half of the total plant area[A] per unit ground surface area ($m^2\,m^{-2}$), and thus it is related to the canopy characteristics. It is an important biophysical parameter in climatic, ecological and agronomical research studies (e.g. Stroppiana *et al*. 2006). User-defined *LAI* values can be obtained from *in situ* measurements or alternatively from landcover maps derived from remote-sensing imagery. However, the reference values shown in Table 3 are also provided by ADM as default for several biomes. These average *LAI* values, and the respective standard deviation values, are derived from the data compilation and statistical analysis performed by Asner *et al*. (2003).

For the simulation of the air flow above the canopy, the wind profile is given by:

$$\frac{k}{u_*} U(z) = \ln\left(\frac{z + d_t}{z_{0m}}\right) - \psi_m\left(\frac{z + d_t}{L}\right) + \psi_m\left(\frac{z_{0m}}{L}\right) + \hat{\psi}_m(z) \quad (\text{for } z<0) \tag{4}$$

where k is the Von Karman's constant (0.41). The expressions for the calculation of the functions ψ_m and $\hat{\psi}_m$ and the roughness length associated with the flow in the inertial sublayer (z_{0m}) are those derived by Physick and Garratt (1995) and Harman and Finnigan (2007). These formulations quantify the deviation from the standard Monin–Obukhov Similarity Theory (MOST) (Monin and Yaglom 1971) profiles, which provide a consistent set of flux–profile relationships for application in the atmospheric surface layer but fail in a layer extending to several canopy heights (Raupach and Thom 1981; Högström 1996), owing to the presence of the canopy. The Obukhov length, L, which is used to characterise the atmospheric stability of the boundary layer, is estimated applying the approach implemented in the meteorological preprocessor AERMET from the air-quality dispersion model AERMOD (for details see US EPA 2004).

Liquid discharge

The second module calculates the variation of flow rate during discharge, i.e. the volume of product released per unit of time, which is a parameter that influences the characteristics of the ground pattern, namely its length and coverage levels. The model also allows the user to provide an input file with measured values of flow rate for the particular discharge system being used. The three systems currently in use in aerial firefighting operations are the Conventional Aerial Delivery System, the Constant Flow Delivery System, and the Modular Aerial Fire Fighting System (MAFFS). In pressurised systems such as MAFFS, information on up to five representative classes of droplet diameters produced by the atomiser is required from the user. Additionally, if measured flow rate is not available for conventional gating systems, ADM offers the possibility to simulate the outflow of liquid from the tank applying the numerical concepts from Swanson *et al*. (1975, 1977) (extensively validated by Swanson *et al*. 1978), as hereafter briefly described. This approach bases the flow-rate prediction on tank geometry and door-opening rate, which have been shown to account for most aspects of tank flow (Swanson *et al*. 1978).

In a truly free-fall tank, the outflow of the liquid from the aircraft changes from acceleration-dominated to steady-state towards the end of discharge. In tanks with only minor flow restrictions and fast doors, the fluid continually accelerates out of the tank; in contrast, in those with sufficient flow restrictions, a steady-state flow is reached and sustained during the discharge. Without the complexity of dealing directly with the equations governing the vertical flow from the tank, numerical approximations are applied in these two flow regimes occurring during the discharge. In general, if the door opening rate has been identified by the model as being fast enough not to restrict the outflow, the model does not allow the steady-state case to be applied.

The model calculates the variation of the acceleration-dominated vertical velocity (w_{Ac}) in each computational time-step from the expression:

$$w_{Ac} = w_E + \Delta t\left(g + \frac{P}{\rho h_L}\right) \tag{5}$$

[A]The plant area corresponds to the leaf area in the case of deciduous canopies and to the needle area in the case of coniferous canopies.

where w_E is the efflux velocity in the previous time-step (at $t = 0\,s \Rightarrow w_E = 0\,\mathrm{m\,s^{-1}}$), g is the acceleration of gravity, ρ the mass density of the liquid, h_L the fluid height, and P the pressure. The steady-state flow is assumed to be described by the Bernoulli equation:

$$w_B = \sqrt{\frac{2g\rho h + 2P}{\rho} + w_t^2} \tag{6}$$

where w_B is the Bernoulli velocity and w_t is the velocity at the top surface of the fluid volume inside the tank. In each time-step, ADM will then calculate the effective area of efflux, which is dependent on the angle between the door and the bottom of the tank. These data can be given by the user or estimated from the model based on the empirical correlations from Swanson *et al*. (1977). Finally, the incremental quantity of retardant released per time-step derives from the calculated velocity of efflux and the effective area. At each computational time-step, the model gives the following output data: head height, exit velocity, top velocity, flow rate, volume discharged per time-step, cumulative volume and pressure.

Liquid breakup

In the third module, ADM applies a set of numerical procedures for the description of the two-stage aerodynamic breakup of the liquid jet. The computational algorithm describing the primary breakup of the jet derives from the jet stability theory applied in the simulation of fuel injection systems in the automotive industry (for details see, e.g. Reitz and Bracco 1982; Reitz 1987; Lin and Reitz 1998; Beale and Reitz 1999). The sizes of the child droplets resulting from primary breakup are thus obtained from the wavelengths of the most unstable waves. The breakup length, however, is a measure of the growth rate of the disturbance. The jet stability theory has been extensively applied and validated by several authors within a wide range of operating conditions. This shows the robustness of the implicit concept (e.g. Lee and Park 2002; Madabhushi 2003; Raju 2005).

The initial conditions for the jet breakup simulation are the flow rate of liquid, the injection velocity, and the characteristic dimensions of the liquid parcels (the initial diameter is imposed as equal to the effective discharge diameter). They are given by the liquid discharge module described earlier. The radius (R) of the droplets stripped from the unstable surface of the jet by Kelvin–Helmholtz (KH) and Rayleigh–Taylor (RT) instabilities, respectively R_{KH} and R_{RT}, is given by:

$$\begin{cases} R_{\mathrm{KH}} = 5.5 \cdot R_{jet} \cdot \dfrac{(1 + 0.45 \cdot Oh_L^{0.5}) \cdot (1 + 0.4 \cdot Ta^{0.7})}{(1 + 0.87 \cdot We_G^{1.67})^{0.6}} \\ R_{\mathrm{RT}} = 0.3 \cdot \pi \sqrt{\left(\dfrac{3 \cdot \sigma}{-(g + a) \cdot (\rho_L - \rho_G)}\right)} \end{cases} \tag{7}$$

where *Oh*, *Ta* and *We* are respectively the Ohnesorge, Taylor and Weber numbers (dimensionless), σ is the surface tension and a is the acceleration of the fluid parcel.

Droplet formation rate, i.e. the volume atomised in each time-step by KH and RT instabilities, is calculated as follows:

$$\begin{cases} V_{\mathrm{atomised\_KH}_{(i)}} = V_{p_{(i-1)}} - \pi \cdot L_{p_{(i-1)}} \cdot R_{p_{(i)}}^2 \\ V_{\mathrm{atomised\_RT}_{(i)}} = \dfrac{\Delta t \cdot k_2 \cdot e^{(k_1 \cdot t)}}{u_p \cdot V_{p_{(i-1)}}} \end{cases} \tag{8}$$

where i indicates the current time-step and $i - 1$ the previous one. L_p, R_p and V_p are respectively the length, radius and volume of the parent liquid parcel before break-up by KH instabilities. L_p and R_p are calculated from the resolution of Eqn 9 (applying a fourth-order Runge–Kutta method), which formulates a uniform radius reduction rate of R_p:

$$\frac{dR_p}{dt} = -\frac{(R_p - R_{\mathrm{KH}})}{\tau_{\mathrm{KH}}}\,,\ R_{\mathrm{KH}} \leq R_p \tag{9}$$

In this equation τ is the breakup time, which is calculated as proposed by Beale and Reitz (1999). However, the calculation of the volume atomised by RT instabilities derives from the extensive work carried out by Swanson *et al*. (1975, 1977, 1978), representing a deviation from the typical linear stability theory. Returning to Eqn 8, u_p is thus the velocity of the fluid parcel (calculated from the deposition module) and k_1 and k_2 are empirical erosion constants; k_1 equals 3.97 in the case of gum-thickened retardants and 4.4 in unthickened products, whereas k_2 has been defined as 12.

In order to optimise the computational run-time, only a fraction of the total number of droplets originating from primary breakup mechanisms is tracked during the computation. Hence, a minimum of 1 and a maximum of 10 marker (or representative) droplets are allowed to be produced per time-step from the atomisation of each individual liquid parcel. This computational feature does not have a significant influence on results and balances the need for adequate representation of the spray while keeping the computational time within practical limits (see, e.g. Crowe *et al*. 1998).

The droplets formed after the primary breakup of the liquid jet column will deform and eventually break up after a given time period, which is calculated from experimental correlations based on the non-dimensional numbers of Weber and Ohnesorge (e.g. Madabhushi 2003). The secondary breakup will occur by one of the two following mechanisms: bag breakup for Weber numbers lower than 100, and shear breakup in the other cases. While in the first case the droplet is assumed to be atomised into five child droplets, in the second, the child droplets are continuously stripped from the parent droplet until its extinction. In the case of bag breakup, the droplet size distribution is assumed to follow the root-normal distribution as originally proposed by Simmons (1977) (and extensively validated after by, for example, Hsiang and Faeth 1995), whereas in the shear breakup process, it is fitted with the Rosin–Rammler expression, which is a distribution widely applied in spray modelling studies (Liu 2000).

Liquid deposition and retention

During breakup, the trajectories of the formed droplets are simulated by integrating the motion equation in a Lagrangian

reference frame, which specifies that the rate of change of linear momentum is equal to the net sum of the forces acting on the droplet. The force balance expressing the dynamical interaction between the liquid and the atmospheric flow field can thus be written as follows (e.g. Crowe *et al*. 1998):

$$\frac{d\vec{U}_L}{dt} = \left(\frac{18\mu_G c_D Re}{24\rho_L D_L^2}\right) \cdot \left(\vec{U}_G - \vec{U}_L\right) + \vec{g} \qquad (10)$$

The subscript L refers to both the primary and secondary child droplets. In this expression, the first term on the right side relates the drag factor to the response time of the droplet; μ_G is the molecular viscosity of the air; c_D is the drag coefficient; ρ_L and D_L are the density and diameter of the droplet; Re is the relative Reynolds number; $\vec{U}_G$ and $\vec{U}_L$ represent the velocity vectors of the continuous phase and the droplet respectively, and $\vec{g}$ is the acceleration due to gravity.

Owing to the droplets' large size, and consequently their inertia, they will behave as nearly unresponsive to turbulent velocity fluctuations. As a consequence, the effects of turbulence on droplet movement are not significant in general, except for the range of smaller diameters that can potentially follow the airflow more closely. As result of the low relative importance of smaller droplets and the interest in keeping the computational time to a manageable level, the turbulent fluctuations of the gaseous phase, and their effects on particle motion, are not taken into account.

Integration in time of Eqn 10 yields the velocity of the particle along the trajectory, whereas the trajectory itself (position of the droplet in each Cartesian coordinate) is given by:

$$\frac{d\vec{X}}{dt} = \vec{U}_L \qquad (11)$$

where $\vec{X}$ is the vector of spatial coordinates, i.e. the position. A fourth-order Runge–Kutta integration method is applied in the solving of Eqns 10 and 11. A time-step of 0.02 s guarantees the needed accuracy without compromising the run-time.

During free-fall, the droplets typically deform into an oblate spheroid. ADM calculates the increase of droplet frontal diameter during the deformation period following the proposal of Hsiang and Faeth (1992) and Madabhushi (2003):

$$D_L = D_{L0} \cdot \left(1 + 0.19 \cdot \sqrt{We} \cdot \frac{t}{t_d}\right) \qquad (12)$$

where D_{L0} is the droplet diameter before deformation, t is current time and t_d is the deformation time (which accounts for the effects of liquid viscosity on breakup time as given by Hsiang and Faeth 1992).

Then, in order to evaluate the effect of non-sphericity over the drag of the free-falling droplets, ADM incorporates the dynamical drag model of Morsi and Alexander (1972), for spherical droplets, and that of Haider and Levenspiel (1989) when the shape is identified as non-spherical.

The suppression effectiveness of firefighting products depends both on the amount of material deposited on a unit area of the fuel, and on the amount of fuel coated by the material (Andersen *et al*. 1974*a*). It is thus important to have a prediction of the vertical distribution of product within the canopy. The penetration of retardant into the canopy, the foliar interception (the fraction of fluid contacting the foliage) and the foliar retention (the fraction retained) have been scarcely investigated in the literature (see, e.g. Calogine *et al*. 2007). With this purpose, an analogy with rainfall interception studies is therefore established. The vertical distribution of retained liquid is estimated by ADM using the film thickness concept of Grah and Wilson (1944), which gives the liquid depth on the surface of leaves after precipitation has ceased and drainage stopped and thus expresses the limit of retention by the fuels. The model will basically assume that the amount of fluid retained in the tree is then given by an equivalent film thickness uniformly applied over the tree surface area. An approximate value for the variation of volume retained with height is then calculated from the knowledge of the vertical profile of *LAI* for the specific canopy considered.

Conclusions

The main objective of the current investigation was the development of the numerical model ADM, which is intended for the unsteady-state simulation of the aerial drop of firefighting agents (water and chemical retardants) by fixed-wing delivery systems operating within typical operational conditions.

The model covers the most important stages in the process, namely, the canopy-induced wind flow; the outflow of the liquid from the aircraft tank; the jet column bending and fracture; the primary breakup of the jet surface and column; the shape distortion and secondary breakup of the formed droplets; the gravitational settling of the droplets; and, finally, the ground deposition of the product. Compared with previous aerial drop models, ADM is capable of providing an enhanced understanding on the aerodynamic breakup of the bulk liquid, which is the most important factor influencing the final spatial distribution of liquid on the ground. This is accomplished by applying an adapted version of the linear stability theory in the numerical description of primary and secondary breakup processes. Although this method is specifically suited for fluids exhibiting Newtonian behaviour, which is not the case for chemical retardants, it provided good results for the range of products evaluated in Part II (Amorim 2011) of this work. The option for this approach is a compromise between modelling accuracy and the fast-running capabilities of the code, given the current state of knowledge on the aerodynamic breakup of non-Newtonian liquids.

For simplicity, the code does not include the effect of thermally induced air motions on the product's behaviour. Therefore, it is specially indicated for 'indirect attack', in which the drop is made at some distance from the fire front, or for effectiveness studies, in which drops are made over bare ground in the absence of fire. However, the code allows the effect over the vertical wind profile induced by a homogeneous vegetative canopy to be considered, fulfilling one of the gaps of previous models.

The wake produced by the aircraft fuselage and propellers is not taken into account by the model. Additional research on the

aircraft wake effect over the ground pattern (due to the disturbed motion of smaller droplets) is needed, in particular for pressurised delivery systems. Also, ADM is not suited for rotary-wing aircraft because it does not consider the downforce caused by the rotor blades, and its effect on breakup and droplets motion.

The main output of ADM is the spatial distribution of the ground concentration of the agent. Additionally, the model provides detailed information on the 3-D position and characteristics of the liquid with time, and several metrics of interest (e.g. line length and area per coverage level) that allow the evaluation of delivery performance as a result of meteorological conditions, flight parameters and product characteristics.

In the operational field, the model may assist in the optimisation of firefighting operations, and the improvement of aerial delivery performance. The user control over the input parameters allows the effect on ground pattern to be assessed for a wide range of release scenarios, avoiding the natural variability and irreproducibility of field conditions, and a complementary understanding of the multiple interrelated phenomena involved. In this sense, this tool could also contribute to reducing the cost of exhaustive real-scale drop testing. Additionally, the fast-running capabilities of the computational code allow it to be used in training and demonstration activities with pilots, aerial resource coordinators, civil protection personnel and ground firefighters.

Acknowledgements

The author is grateful to his PhD supervisor Prof Carlos Borrego, and to all colleagues from the Research Group on Emissions, Modelling and Climate Change (GEMAC) at the University of Aveiro (Portugal); to engineer Ryan Becker (San Dimas Technology and Development Center, USDA-FS); to Dr Ian Harman (CSIRO Marine and Atmospheric Research, Australia); and to Prof Rolf Reitz (University of Wisconsin, US). The author acknowledges the helpful corrections and questions raised by the reviewers. This work was partly supported by the Foundation for Science and Technology, from the Portuguese Ministry of Science, Technology and Higher Education, through the PhD grant (SFRH/BD/11044/2002), a post-doctoral grant (SFRH/BPD/48121/2008) and the national research projects INTERFACE (POCI/AMB/60660/2004) and FUMEXP (FCOMP-01-0124-FEDER-007023), and by the European Commission through the research projects ERAS (EVG1-2001-00019) and EUFIRELAB (EVR1-CT-2002-40028). Also financial support of the Luso–American Foundation (FLAD) is acknowledged.

References

Amorim JH (2008) Numerical modelling of the aerial drop of products for forest firefighting. PhD Thesis, University of Aveiro, Portugal.

Amorim JH (2011) Numerical modelling of the aerial drop of products for forest firefighting. Part II: model validation. *International Journal of Wildland Fire* **20**, 394–406. doi:10.1071/WF09123

Amorim JH, Miranda AI, Borrego C, Varela V (2006) Recent developments on retardant aerial drop modelling for operational purposes. In 'Proceedings of the 5th International Conference on Forest Fire Research', 27–30 November 2006, Figueira da Foz, Portugal. (Ed. DX Viegas) (CD-ROM) (Millpress: Rotterdam)

Andersen WH, Brown RE, Kato KG, Louie NA (1974*a*) Investigation of rheological properties of aerial-delivered fire retardant – Final report. USDA Forest Service, Intermountain Research Station, Report 8990-04. (Ogden, UT)

Andersen WH, Brown RE, Louie NA, Blatz PJ, Burchfield JA (1974*b*) Investigation of rheological properties of aerial-delivered fire retardant extended study – Final report. USDA Forest Service, Intermountain Research Station, Report 8990-05. (Ogden, UT)

Andersen WH, Brown RE, Louie NA, Kato KG, Burchfield JA, Dalby JD, Zernow L (1976) Correlation of rheological properties of liquid fire retardant with aerially delivered performance – Final report. USDA Forest Service, Intermountain Research Station, Report 8990-08. (Ogden, UT)

Asner GP, Scurlock JMO, Hicke JA (2003) Global synthesis of leaf area index observations: implications for ecological and remote sensing studies. *Global Ecology and Biogeography* **12**, 191–205. doi:10.1046/J.1466-822X.2003.00026.X

Beale JC, Reitz RD (1999) Modeling spray atomization with the Kelvin–Helmholtz/Rayleigh–Taylor hybrid model. *Atomization and Sprays* **9**, 623–650.

Belcher SE, Jerram N, Hunt JCR (2003) Adjustment of a turbulent boundary layer to a canopy of roughness elements. *Journal of Fluid Mechanics* **488**, 369–398. doi:10.1017/S0022112003005019

Calogine D, Rimbert N, Séro-Guillaume O (2007) Modelling of the deposition of retardant in a tree crown during fire fighting. *Environmental Modelling & Software* **22**, 1654–1666. doi:10.1016/J.ENVSOFT.2007.01.003

Cescatti A, Marcolla B (2004) Drag coefficient and turbulence intensity in conifer canopies. *Agricultural and Forest Meteorology* **121**, 197–206. doi:10.1016/J.AGRFORMET.2003.08.028

Crowe C, Sommerfeld M, Tsuji Y (1998) 'Multiphase Flows with Droplets and Particles.' (CRC Press: Florida)

Finney MA (1998) FARSITE: Fire Area Simulator – model development and evaluation. USDA Forest Service, Rocky Mountain Research Station, Research Paper RMRS-RP-4. (Ogden, UT)

Finnigan J (2000) Turbulence in plant canopies. *Annual Review of Fluid Mechanics* **32**, 519–571. doi:10.1146/ANNUREV.FLUID.32.1.519

Finnigan JJ, Brunet Y (1995) Turbulent airflow in forests on flat and hilly terrain. In 'Wind and Trees'. (Eds MP Coutts, J Grace) pp. 3–40. (Cambridge University Press: Cambridge, UK)

George CW, Blakely AD (1973) An evaluation of the drop characteristics and ground distribution patterns of forest fire retardants. USDA Forest Service, Intermountain Research Station, Research Paper INT-134. (Ogden, UT)

George CW, Johnson GM (1990) Developing air tanker performance guides. USDA Forest Service, Intermountain Research Station, General Technical Report INT-268. (Ogden, UT)

Giménez A, Pastor E, Zárate L, Planas E, Arnaldos J (2004) Long-term forest fire retardants: a review of quality, effectiveness, application and environmental considerations. *International Journal of Wildland Fire* **13**, 1–15. doi:10.1071/WF03001

Grah RA, Wilson CC (1944) Some components of rainfall interception. *Journal of Forestry* **42**, 890–898.

Haider A, Levenspiel O (1989) Drag coefficient and terminal velocity of spherical and non-spherical particles. *Powder Technology* **58**, 63–70. doi:10.1016/0032-5910(89)80008-7

Harman I, Finnigan J (2007) A simple unified theory for flow in the canopy and roughness sublayer. *Boundary-Layer Meteorology* **123**, 339–363. doi:10.1007/S10546-006-9145-6

Högström U (1996) Review of some basic characteristics of the atmospheric surface layer. *Boundary-Layer Meteorology* **78**, 215–246. doi:10.1007/BF00120937

Hsiang L-P, Faeth GM (1992) Near-limit drop deformation and secondary breakup. *International Journal of Multiphase Flow* **18**, 635–652. doi:10.1016/0301-9322(92)90036-G

Hsiang L-P, Faeth GM (1995) Drop deformation and breakup due to shock wave and steady disturbances. *International Journal of Multiphase Flow* **21**, 545–560. doi:10.1016/0301-9322(94)00095-2

Inoue E (1963) The environment of plant surfaces. In 'Environment Control of Plant Growth'. (Ed. LT Evans) pp. 23–32. (Academic Press: New York)

IPCC (2007) 'Climate Change 2007: Synthesis Report. Contribution of Working Groups I, II and III to the Fourth Assessment Report of the Intergovernmental Panel on Climate Change.' (Eds RK Pachauri, A Reisinger) (Intergovernmental Panel on Climate Change: Geneva)

Lee CS, Park SW (2002) An experimental and numerical study on fuel atomization characteristics of high-pressure diesel injection sprays. *Fuel* **81**, 2417–2423. doi:10.1016/S0016-2361(02)00158-8

Lin SP, Reitz RD (1998) Drop and spray formation from a liquid jet. *Annual Review of Fluid Mechanics* **30**, 85–105. doi:10.1146/ANNUREV.FLUID.30.1.85

Linne MA, Paciaroni M, Gord JR, Meyer TR (2005) Ballistic imaging of the liquid core for a steady jet in crossflow. *Applied Optics* **44**, 6627–6634. doi:10.1364/AO.44.006627

Liu H (2000) 'Science and Engineering of Droplets: Fundamentals and Applications.' (William Andrew Inc.: New York)

Madabhushi RK (2003) A model for numerical simulation of breakup of a liquid jet in crossflow. *Atomization and Sprays* **13**, 413–424. doi:10.1615/ATOMIZSPR.V13.I4.50

Monin AS, Yaglom AM (1971) 'Statistical Fluid Mechanics: Mechanisms of Turbulence – Vol. 1.' (The Massachusetts Institute of Technology (MIT) Press: Cambridge, MA, USA)

Morsi SA, Alexander AJ (1972) An investigation of particle trajectories in two-phase flow systems. *Journal of Fluid Mechanics* **55**, 193–208. doi:10.1017/S0022112072001806

Novak MD, Warland JS, Orchansky AL, Ketler R, Green S (2000) Wind tunnel and field measurements of turbulent flow in forests. Part 1: uniformly thinned stands. *Boundary-Layer Meteorology* **95**, 457–495. doi:10.1023/A:1002693625637

Physick WL, Garratt JR (1995) Incorporation of a high-roughness lower boundary into a mesoscale model for studies of dry deposition over complex terrain. *Boundary-Layer Meteorology* **74**, 55–71. doi:10.1007/BF00715710

Raju MS (2005) Numerical investigation of various atomization models in the modeling of a spray flame. National Aeronautics and Space Administration (NASA) Report E-15389. (Washington, DC) Available at http://gltrs.grc.nasa.gov/reports/2005/CR-2005-214033.pdf [Verified 23 March 2011]

Raupach MR, Thom AS (1981) Turbulence in and above plant canopies. *Annual Review of Fluid Mechanics* **13**, 97–129. doi:10.1146/ANNUREV.FL.13.010181.000525

Reitz RD (1987) Modeling atomization processes in high-pressure vaporizing sprays. *Atomization and Spray Technology* **3**, 309–337.

Reitz RD, Bracco FV (1982) Mechanism of atomization of a liquid jet. *Physics of Fluids* **25**, 1730–1742. doi:10.1063/1.863650

Rimbert N, Calogine D, Séro-Guillaume O (2002) Modelling of retardant dropping and atomisation. In 'Proceedings of the 4th International Conference on Forest Fire Research', 18–23 November 2002, Luso, Coimbra, Portugal. (Ed. DX Viegas) (CD-ROM) (Millpress: Rotterdam)

Séro-Guillaume O, Rimbert N (2005) On thermodynamic closures for two-phase flow with interfacial area concentration transport equation. *International Journal of Multiphase Flow* **31**, 897–920. doi:10.1016/J.IJMULTIPHASEFLOW.2005.05.005

Simmons HC (1977) The correlation of drop-size distribution in fuel-nozzle sprays. *Journal of Engineering for Gas Turbines and Power* **99**, 309–319.

Stroppiana D, Boschetti M, Confalonieri R, Bocchi S, Brivio PA (2006) Evaluation of LAI-2000 for leaf area index monitoring in paddy rice. *Field Crops Research* **99**, 167–170. doi:10.1016/J.FCR.2006.04.002

Swanson DH, Helvig TN (1973) High-altitude retardant drop mechanization study. Honeywell Inc., Government and Aeronautical Products Division, Final Report, Vol. 1, Contract 26-2888. (Hopkins, MI)

Swanson DH, Helvig TN (1974) Extended high-altitude retardant drop mechanization study. Honeywell Inc., Government and Aeronautical Products Division. Final Report, Contract 26-2888. (Hopkins, MI)

Swanson DH, Luedecke AD, Helvig TN, Parduhn FJ (1975) Development of user guidelines for selected retardant aircraft. Final Report, Contract 26–3332. Honeywell Inc., Government and Aeronautical Products Division. (Hopkins, MI)

Swanson DH, Luedecke AD, Helvig TN, Parduhn FJ (1977) Supplement to development of user guidelines for selected retardant aircraft. Honeywell Inc., Government and Aeronautical Products Division, Final Report, Contract 26-3332. (Hopkins, MI)

Swanson DH, Luedecke AD, Helvig TN (1978) Experimental tank and gating system (ETAGS). Honeywell Inc., Government and Aeronautical Products Division, Final Report, Contract 26-3425. (Hopkins, MI)

Teske ME, Bird SL, Esterly DM, Ray SL, Perry SG (1997) A user's guide for AgDRIFT 1.0: a tiered approach for the assessment of spray drift of pesticides. Continuum Dynamics, Inc., Technical Note 95-10. (Princeton, NJ)

Teske ME, Kaufman AE, Johnson GM (1999) Collapsing bucket drop test data with a Lagrangian model. In 'Proceedings of the 12th Annual Conference on Liquid Atomization and Spray Systems (ICLASS)', May 1999, Indianapolis, IN. (Institute for Liquid Atomization and Spray Systems (ILASS): Irvine, CA)

Tomé M (2004) Modelação da nuvem de retardante químico: optimização no combate aos fogos florestais. PhD dissertation, University of Aveiro, Portugal.

Tomé M, Borrego C (2002) Fighting wildfires with retardants applied with airplanes. In 'Proceedings of the 4th International Conference on Forest Fire Research', 18–23 November 2002, Luso, Coimbra, Portugal. (Ed. DX Viegas) (CD-ROM) (Millpress: Rotterdam)

US EPA (2004) User's guide for the AERMOD meteorological preprocessor (AERMET) – Revised draft. US Environmental Protection Agency (US EPA), Office of Air Quality Planning and Standards Report EPA-454/B-03-002. (Research Triangle Park, NC)

Westerling AL, Hidalgo HG, Cayan DR, Swetnam TW (2006) Warming and earlier spring increase Western US forest wildfire activity. *Science* **313**, 940–943. doi:10.1126/SCIENCE.1128834

WHO (2007) 'The World Health Report 2007 – A Safer Future: Global Public Health Security in the 21st Century.' (World Health Organization: Geneva)

Manuscript received 30 October 2009, accepted 27 July 2010

Appendix. Nomenclature used in this paper

Variables

- a, acceleration of the liquid agent parcel (m s^{-2})
- c_D, drag coefficient (unitless)
- C, concentration of agent at ground (L m^{-2} or gpc)
- C_z, variation with height of concentration (L m^{-2} or gpc)
- d_t, displacement height (m)
- D_L, droplet diameter (m or mm)
- D_V, equivalent vent diameter (m)
- g, gravitational acceleration (m s^{-2})
- h, canopy average height (m)
- h_L, fluid height in the tank (m)
- H_a, drop height (m)
- H_T, tank height (m)
- H_m, meteorological parameters measurement height (m)
- k, von Karman's constant (unitless)
- L, Obukhov length (m)
- L_c, canopy-drag length scale (m)
- L_D, tank doors length (m)
- L_p, parent droplet length (m)
- L_T, tank length (m)
- L_V, vent length (m)
- LAI, cumulative leaf area index at ground (m^2 m^{-2})
- Oh, Ohnesorge number $(\mu/\sqrt{\sigma\rho L})$ (unitless)
- P, pressure (Pa)
- Q, flow rate of liquid discharged (m^3 s^{-1})
- Q_t, variation with time of flow rate of liquid discharged (m^3 s^{-1})
- Re, Reynolds number ($UL\rho/\mu$) (unitless)
- R, droplet radius (m)
- R_p, parent droplet radius (m)
- t, time (s)
- t_α, door opening time (s)
- Ta, Taylor number $(Oh_L\sqrt{We_G})$ (unitless)
- u, v, w, fluid velocity components in Cartesian coordinates (m s^{-1})
- u_p, parent droplet velocity (m s^{-1})
- u_*, friction velocity (m s^{-1})
- u_{Lt}, v_{Lt}, w_{Lt}, variation with time of velocity (m)
- U, fluid (air or liquid) velocity (m s^{-1})
- U_a, aircraft velocity (m s^{-1})
- U_h, wind velocity at canopy top (m s^{-1})
- U_m, wind velocity measured at height H_m (m s^{-1})
- V_L, volume of fluid dropped (m^3)
- V_p, parent droplet volume (m^3)
- w_{Ac}, acceleration-dominated velocity (m s^{-1})
- w_B, Bernoulli velocity (m s^{-1})
- w_E, efflux vertical velocity (m s^{-1})
- w_t, fluid velocity at the top (m s^{-1})
- We, Weber number ($\rho U^2 L/\sigma$) (unitless)
- W_D, tank doors width (m)
- W_T, tank width (m)
- x, y, z, Cartesian coordinates (m)
- x, fluid position (m)
- x_{Lt}, y_{Lt}, z_{Lt}, variation with time of position (m s^{-1})
- z, height (m)
- z_{0m}, roughness length (m)

Greek variables

- α_D, door opening angle (°)
- β, canopy parameter (unitless)
- Δt, liquid discharge time (s)
- θ_a, aircraft direction (in meteorological coordinates) (°)
- θ_m, wind direction (meteorological coordinates) measured at height H_m (°)
- μ, dynamic viscosity (Pa s or cP)
- ρ, mass density (kg m^{-3})
- σ, surface tension (N m^{-1})
- ψ_m, integrated form of the similarity function (unitless)

Overlines

Where X is used only to show position of overlines.

- $\hat{X}$, roughness sublayer (RSL) variable
- $\vec{X}$, Vector

Subscripts

Where X is used only to show position of subscript.

- X_D, aircraft tank doors
- X_G, gas phase
- X_{KH}, Kelvin–Helmholtz instability
- X_L, liquid phase
- X_m, measured value
- X_{RT}, Rayleigh–Taylor instability
- X_T, aircraft tank
- X_0, initial value